2010년 2월
박사학위논문

A role of RRM3 for the regulation of intracellular reactive oxygen species in response to UV irradiation

조선대학교 대학원

의학과

문 재 원

A role of RRM3 for the regulation of intracellular reactive oxygen species in response to UV irradiation

자외선 조사에 의하여 생성되는 세포내 활성산소 조절에 관여하는 RRM3의 역할

2010년 **2** 월 **25** 일

조선대학교 대학원

의학과

문 재 원

A role of RRM3 for the regulation of intracellular reactive oxygen species in response to UV irradiation

지도교수 양 정 열

이 논문을 의학박사 학위신청논문으로 제출함.

2009년 10월 일

조선대학교 대학원

의학과

문 재 원

문재원의 박사학위논문을 인준함

위원장　조선 대학교　교수　김철성　인

위　원　조선 대학교　교수　양정열　인

위　원　조선 대학교　교수　유호진　인

위　원　조선 대학교　교수　장인엽　인

위　원　조선 대학교　교수　천지선　인

2009년 12월　일

조선대학교 대학원

CONTENTS

ABSTRACT

자외선 조사에 의하여 생성되는 세포내 활성산소 조절에 관여하는 RRM3의 역할

문 재 원
지도교수: 양 정 열
의학과
조선대학교 대학원

p53에 의하여 발현이 조절되는 RRM3는 세포 내에서 활성산소 생성을 증가시켜 세포 사멸사를 유도하는 것으로 알려져 있으나 RRM3에 의한 활성산소 생성 기작은 아직 규명되지 못하였다. 본 연구에서는 RRM3에 의한 활성산소 생성 기작을 규명하기 위하여, RRM3와 결합하는 항산화제를 탐색하여 활성산소 중 과산화수소를 제거하는 catalase가 RRM3와 결합함을 yeast two hybridization 방법으로 발견하였다. RRM3와 catalase의 결합은 자외선 조사에 의하여 현저하게 증가 함을 co-immunoprecipitation 및 면역형광법에 의하여 확인하려 하였다. 또한 분리한 RRM3 및 catalase 단백질을 사용하여 두 단백질이 직접 결합함을 규명하였다. RRM3를 과발현시키면 세포의 catalase활성이 감소되고 활성산소가 증가하였으며, 반면에 RRM3를 siRNA로 결핍시키면 세포내 catalase 활성이 증가하고 활성산소 생성이 감소하였다. RRM3과발현 세포에 자외선을 조사하면 catalase활성이 현저하게 감소되고 활성산소가 증가하여 세포 사멸사가 대조세포에

비하여 현저하게 증가되었으며 이들 세포에 catalase를 과발현시키면 RRM3에 의한 세포 사멸사가 현저하게 감소하였다. 따라서 RRM3는 사람세포에서 catalase활성을 감소시켜 활성산소를 생성하고 세포사멸사를 유발하는 것으로 판단되었다.

I. INTRODUCTION

The p53 protein functions as a sequence-specific DNA-binding factor that can activate genes whose promoters contain a p53 response element (1-2). In response to various genotoxic stresses and oncogenic stimuli, p53 is subjected to a number of post-translation modification, including phosphorylation and acetylation, which promote DNA binding and translational activation (3). A number of genes involved in control of cell cycle and apoptosis are regulated by p53. By using serial analysis of gene expression (SAGE) technique to evaluate the patterns of gene expression following p53 expression, a series of p53-induced genes (PIGs) have been identified that are predicted to encode proteins that could generate or respond to oxidative stress (4). Some PIGs encode factors that induce the intracellular accumulation of reactive oxygen species (ROS). One such gene is the p53-inducible gene 3 (RRM3). p53 interacts with a pentanucleotide microsatellite sequence within the *RRM3* promoter [$(TGYCC)_n$, where Y=C or T] that is required for transcriptional activation of this promoter by p53 (5). RRM3 expression can also be elicited by p63 and p53 (6), which are able to induce apoptosis in a p53-independent manner (7). The RRM3 amino acid sequence shows significant homology to that of NADPH quinine oxidoreductase1 (NQO1), suggesting that, like NQO1, RRM3 contributes to the generation of reactive oxygen species (ROS) (4), which are important downstream mediators of the p53-dependent apoptotic response. Additionally, p53 mutants that selectively fail to induce apoptosis but not cell cycle arrest also fail to activate RRM3 but not other p53-responsive genes (8-10). Moreover, human cellular apoptosis susceptibility protein (hCAS/CSE1L) interacts with the *RRM3* promoter and affects p53-dependent

apoptosis by regulating RRM3 expression (11). Therefore, It is likely that RRM3 is involved in the p53-induced apoptosis through generation of intracellular ROS. However, the exact role of RRM3 in p53-dependent apoptosis and the detailed mechanism of the RRM3-mediated ROS generation remain to be determined.

ROS are produced as a by-product of cellular metabolism and exposure to ultraviolet light, ionizing radiation, and environmental carcinogens (12-13). Organisms have therefore evolved a series of antioxidant mechanisms to maintain and protect their intracellular redox homeostasis (13-15). Oxidative stress is a biochemical condition that is characterized by the imbalance between the presence of relatively high levels of ROS and the antioxidative defense mechanisms (16). When the balance between oxidants and antioxidants toward the oxidant side, causing induce oxidative damage to marcromolecules, including nucleic acids and proteins, and this can be harmful to cells and induce apoptosis (17) and pathogenesis of human disease (14). To neutralize these ROS, living cells have acquired various defense systems including non-enzymatic (♋-tocopherol, vitamin C) and enzymatic antioxidants. In particular, superoxide anion (O_2^-) is converted to less reactive H_2O_2 and O_2 by superoxide dismutase (SOD). H_2O_2 is converted to H_2O and O_2 either by catalase or glutathione peroxidase.

In the present study, we used a yeast two-hybrid system to identify catalase as a RRM3-binding protein. We found that purified RRM3 protein incubated with purified catalase protein significantly decreased catalase activity in a dose-dependent manner. Additionally, a region between amino acids 1 and 206 of RRM3, which does not bind catalase, only slightly affected catalase activity. Moreover, RRM3 increased UV-stimulated

ROS generation and UV-induced apoptosis by suppressing catalase activity. Our results suggest that RRM3 regulates the intracellular ROS generation and apoptosis by modulating catalase activity.

II. MATERIALS AND METHODS

1.Materials

Reagents were obtained from the following sources: antibodies to catalase, p53, p53-HRP, and p53R2, from Santa Cruz; anti-cleaved caspase-3, anti-cleaved caspase-7, and anti-Puma antibodies, from Cell Signaling; antibody to Bax, from BD Bioscience; antibody to Noxa, from Calbiochem; antibody to the V5 tag, from Invitrogen; antibody to ♋-tubulin, from NeoMarker; anti-rabbit IgG, and anti-goat IgG, from R&D Systems; anti-mouse IgG, from Upstate; peroxidase-conjugated anti-goat, anti-rabbit, and anti-mouse secondary antibodies, from Jackson ImmunoResearch Laboratories; hydrogen peroxide, poly-L-lysine, neomycin, and propidium iodide (PI), from Sigma-Aldrich; protease inhibitor cocktail, from Roche; Amplex Red catalase assay kit, and 5-(and-6)-chloromethyl-2′,7′-dichlorodihydrofluoescein diacetate, acetyl ester (CM-H_2DCFDA), from Molecular Probes; protein G-Sepharose beads, from GE Healthcare; IMDM, EMEM, RPMI 1640 medium, MacCoy's 5A medium, penicillin-streptomycin (PS), and trypsin, from Gibco-BRL; and fetal bovine serum (FBS), from Cambrex.

2. Cell culture

The human colon carcinoma cell lines HCT116 and HCT116 $p53^{-/-}$ were cultured in Iscove's modified Dulbecco's medium (IMDM) with 10% FBS and 1% PS. The human colon carcinoma cell line RKO was grown in Eagle's minimum essential medium (EMEM) with 10% FBS and 1% PS. The human osteosarcoma cell lines U2OS and Saos-2 were cultured in MacCoy's 5A medium with 15% FBS and 1% PS. The human lung carcinoma

cell lines NCI H460 and NCI H1299 were maintained in RPMI 1640 medium with 10% FBS and 1% PS. The human embryonic kidney cell line HEK293T was grown in DMEM with 10% FBS and 1% PS. The HCT116 $p53^{-/-}$ cell line was a gift from Dr. Bert Vogelstein (Johns Hopkins University School of Medicine, Baltimore, MD), and the HEK293T cell line was obtained from the Cornell Institute for Medical Research. All other cell lines were obtained from the American Type Culture Collection (Rockville, MD).

3. UV irradiation

Cells were washed in culture medium, replaced in a minimal volume of serum-free culture medium, and exposed to light from a 254-nm UVC lamp (UVP; Model UVGL-25) at a dose of 10 J/m^2. After exposure, the cells were cultured in serum-containing medium at 37°C for the appropriate times.

4. Immunoprecipitation assay and Western blot analysis

Cells were rinsed once with ice-cold PBS and lysed in ice-cold NP-40 lysis buffer (50 mM Tris-HCl [pH 8.0], 150 mM NaCl, and 1% Nonidet P-40) with one tablet of EDTA-free protease inhibitor cocktail (Roche). The soluble fraction of the cell lysates was isolated by centrifugation at 13,000 × *g* for 20 min in a microfuge. Supernatants were measured for protein concentration using a detergent-compatible protein assay (Bio-Rad), and equal amounts of proteins were separated by 6–15% SDS-PAGE, followed by electrotransfer onto a polyvinylidene difluoride membrane (Millipore, Bedford, MA). The membranes were blocked for 2 h with TBS-t (10 mM Tris-HCl [pH 7.4], 150 mM NaCl, and 0.1% Tween-20) containing 5% non-fat milk at room temperature and then incubated with

primary antibodies overnight at 4 ㅀC. The blots were washed four times for 15 min with TBS-t containing 0.1% Tween 20 and then incubated for 2 h with peroxidase-conjugated secondary antibodies (1:4000) at room temperature. The membranes were washed four more times and developed using an enhanced chemiluminescence detection system (iNtRON Biotech, Korea). For the immunoprecipitation assay, lysates were precleared with protein G-Sepharose beads prior to adding the primary antibody for 15 min. After removing protein G-Sepharose by centrifugation, supernant was transferred and incubated with primary antibodies for 16 h at 4°C. 20 μl of a 50% slurry of protein G-Sepharose beads were added, and the incubation was continued for an additional 1 h. The immunoprecipitates were washed three times with modified RIPA buffer (25mN Tris [pH 7.2], 150mM NaCl, 5mM $MgCl_2$, 0.5% NP-40, 1mM DTT, and 5% glycerol). Immunoprecipitated proteins were denatured in SDS sample buffer, boiled for 5 min, and analyzed by Western blotting using the appropriate antibodies.

For the in vitro protein binding assay, purified recombinant catalase was incubated with p53, p53R2, Puma, Bax, or Noxa in NP-40 lysis buffer overnight at 4°C. After incubation with antibodies to p53, p53R2, and catalse overnight at 4°C, protein G-Sepharose beads were then added. The beads were washed, and the bound immunocomplexes were analyzed by Western blotting with anti-catalase antibodies.

5. Expression and purification of recombinant proteins

The p53R2 cDNAs were cloned into the His-pET vector via BamHI and XhoI sites. Recombinant 6His-tagged p53R2 protein was expressed in *Escherichia coli* BL21 (DE3) cells after induction with 1 mM IPTG for 6 h in LB-medium at 37°C. The bacterial cells

were collected by centrifugation, resuspended in lysis buffer (20 mM Tris−HCl [pH 7.9], 500 mM NaCl, 5 mM imidazole, 1 mM NaF, and 1 mM PMSF), sonicated, and then centrifuged at 12,000 × *g* at 4°C for 30 min. The recombinant proteins were purified with a Ni−NTA affinity column (Qiagen, Chatsworth, CA), according to the manufacturer's instructions.

Recombinant purified p53 protein was obtained from Calbiochem. Recombinant purified Puma protein was from Bioclone (San Diego, CA). Recombinant purified Bax and Noxa proteins were generous gifts from Dr. T. H. Kim (Chosun University).

6. Plasmid constructs and clones

The cDNA for human wild-type p53 was amplified from GM00637 human fibroblast cells by RT-PCR using the p53 primers ATGGAGGAGCCGCAGTCAGATCCT (sense) and GTCTGAGTCAGGCCCTTCTGTC (antisense). The amplified p53 cDNA construct was cloned into the mammalian expression vector pcDNA3.1/V5-His TOPO (Invitrogen) and confirmed by DNA sequencing. The various truncated p53 cDNA fragments (coding for amino acids 1-300, 1-100, 101-393, 101-300, and 301-393) were PCR-amplified using NOVA-Taq polymerase (Genenmed Inc, Korea), and the resulting PCR products were cloned into pcDNA3.1/V5-His TOPO.

The cDNA for human p53R2 was amplified from GM00637 human fibroblast cells by RT-PCR using the p53R2 primers GAATTCATGGGCGACCCGGAAAGGC (sense) and AAAATCTGCATCCAAGGTGAA (antisense). The amplified p53R2 cDNA construct was cloned into the mammalian expression vector pcDNA3.1/V5-His TOPO (Invitrogen) and confirmed by DNA sequencing. The full-length p53R2 cDNA and various

truncated p53R2 cDNA fragments (coding for amino acids 1-351, 1-160, 1-206, 11-351, and 316-351) were PCR-amplified using NOVA-Taq polymerase (Genenmed Inc, Korea), and the resulting PCR products were cloned into the Gateway Entry vector pENTR/D-TOPO (Invitrogen). The constructs were checked for integrity by sequencing and then used for transfer of the inserts into plasmid pcDNA-DEST47 (C-terminal GFP tag) (Invitrogen) by Gateway LR reactions.

The cDNA for human wild-type catalase was amplified from GM00637 human fibroblast cells by RT-PCR using the catalase primers ATGGCTGACAGCCGGGATCCC (sense) and CAGATTTGCCTTCTCCCTTGCC (antisense). The amplified catalase cDNA construct was cloned into the mammalian expression vector pcDNA3.1/V5-His TOPO (Invitrogen) and confirmed by DNA sequencing. For stable transfection, the catalase expression vector and control vectors were transfected into NCI H1299 cells using Lipofectamine 2000 (Invitrogen), according to the manufacturer's instructions. After transfection, the cells were incubated for 5 weeks in complete medium containing 400 μg/mL neomycin, and the clones resistant to neomycin were isolated and analyzed.

Expression vector pCEP4 HA-Puma was purchased from addgene. The cDNA for hman Bax was amplified from GM00637 human fibroblast cells by RT-PCR using the Bax primer ATGGACGGGTCCGGGGAGC (sense) and GACACGTAAGGAAAACGCATTATAGACCACACT (antisense). The amplified Bax cDNA construct was cloned into the mammalian expression vector pcDNA3.1/V5-His TOPO (Invitrogen). Expression vector pEGFP-C1-hNoxa was a generous gift from Dr. T. H. Kim (Chosun University).

7. Expression of p53, p53R2, and catalase by the adenovirus system

nts were added to fresh HEK293T cells and cultured for 1 week to amplify the adenoviruses. After two to four amplifications, the resulting adenovirus-containing media were used as virus stocks. Viral titers were determined by the plaque-forming assay with HEK293T cells. As a control, pAd/CMV/V5-GW/lacZ vector (Invitrogen) was digested with PacI and transfected into HEK293T cells, to produce lacZ-bearing adenovirus. Aliquots of the adenovirus-containing media were added to cells and cultured for the appropriate periods for subsequent analyses.

8. Small-interference RNA (siRNA) knockdown of p53, p53R2, and catalase

Using the siRNA Target Finder Program (Ambion, Austin, TX), siRNA sequences targeting human p53, p53R2, and catalase were designed. The sequences of the 21-bp siRNA duplexes were: p53, UUACACAUGUAGUUGUAGUGGAUGG (sense strand); p53R2, UGAGUUUGUAGCUGACAGAUU (sense strand); and catalase, UGGAUAUGGAUCACAUACU (sense strand). Control siRNA was from Bioneer (Daejeon, Korea). Cells were transiently transfected with siRNA duplexes using Lipofectamine RNAiMAX (Invitrogen).

9. Measurement of intracellular ROS levels

Intracellular ROS production was assayed using the fluorochrome marker 5-(and-6)-chloromethyl-2′,7′-diclorodihydrofluoescein diacetate, acetyl ester (CM-H_2DCFDA) probe (Invitrogen, Molecular Probes). A fresh stock solution of CM-H_2DCFDA was prepared in DMSO and diluted to a final concentration of 5 μM in 1×

PBS. Cells were washed with 1× PBS, followed by incubation with CM-H_2DCFDA working solution for 30 min in the dark at 37°C. The cells were washed twice and resuspended in PBS, and the increase in fluorescence was detected by flow cytometry (FACSCalibur, BD Biosciences). We analyzed the data with CellQuest software and used the mean fluorescence intensity to quantify responses. The mean fluorescence of 30,000 analyzed cells (corrected for autofluorescence) of each treatment group was taken as a measure of the total ROS load.

10. Assay for catalase activity

Cells were sonicated in 0.1 M Tris-HCl (pH 7.5) for two 30-s bursts. After centrifugation at 12,000 × *g* for 20 min, the supernatants were measured for protein concentration using a detergent-compatible protein assay (Bio-Rad), and catalase activity was measured with an Amplex Red catalase assay kit, according to the manufacturer's protocol (Molecular Probes). After incubating the samples with 40 μM H_2O_2 for 30 min, the remaining H_2O_2 was measured to determine the catalase activity. Amplex Red and horseradish peroxidase react with H_2O_2 to produce resorufin, a fluorescent compound detectable by spectrophotometry. Standard curves for the enzymatic activity of catalase were determined using purified catalase. Enzyme-specific activity was expressed as units/ml of protein, where one unit of catalase activity was defined as 1 μmol H_2O_2 consumed per min.

11. Apoptosis assay

Floating and trypsin-detached cells were collected and washed once with ice-cold PBS, followed by fixing in 70% cold ethanol for 30 min at 4°C. The cells were then washed

with ice-cold PBS, resuspended in PBS containing PI (50 μg/ml), RNase A (100 μg/ml), and 0.1% Triton X-100, and left for 30 min at room temperature. To analyze apoptosis, hypodiploid DNA (sub-G1) populations were assayed using a FACSCalibur flow cytometer with CellQuest software (Becton Dickinson, Franklin Lakes, NJ). The results represent the means of triplicate determinations in which a minimum of 10,000 cells was assayed for each determination. Any sub-G1 populations were counted as apoptotic cells.

12. Immunofluorescence microscopy

U2OS cells treated with 50 J/m^2 UV for 4 h or 50 ❍M H_2O_2 for 12h, or control siRNA- or p53 siRNA-transfected U2OS and RKO cells were cultured on cover slips coated with poly-L-lysine (Sigma) and were then washed twice with PBS, fixed in 4% paraformaldehyde for 10 min, followed by permeabilization with 0.3% Triton X-100 for 15 min at room temperature. Next, the cover slips were washed three times with PBS and then blocked with 5% BSA in PBS for 1 h at room temperature. The cells were double-immunostained with primary antibodies against various proteins overnight at 4°C, after which the cells were washed with PBS and stained with Alexa Fluor 488- (green fluorescence; Molecular Probes) or Alexa Fluor 594- (red fluorescence; Molecular Probes) conjugated secondary antibodies, as appropriate. After washing, the cells were mounted using Vectashield mounting medium with 4,6-diamidino-2-phenylindole (Vector Laboratories, Burlingame, CA). Fluorescence images were taken using a confocal microscope (Zeiss LSM 510 Meta; Carl Zeiss, Jena, Germany) and Zeiss LSM Image Examiner software (Carl Zeiss, Jena, Germany).

13. Yeast two-hybrid analysis

A yeast two-hybrid screen was performed using a Matchmaker GAL4 Two-Hybrid System 3 (Clontech, Mountain View, CA), following the manufacturer's directions. *Saccharomyces cerevisiae* strain AH109, containing distinct ADE2, HIS3, lacZ, and MEL1 reporter constructs, was used for the assay. The AH109 strain was transformed with the bait plasmid pGBT9, encoding an in-frame fusion of the GAL4 DNA-binding domain with full-length p53 or catalase. Transformants were plated onto selective SD medium lacking Trp and incubated for 3−5 days at 30°C. Yeast strains containing the bait plasmid were transformed with a prostate cDNA library fused to the GAL4 activation domain in pACT2 vector. Diploids were plated on SD-Leu/-Trp/-His medium, and growing colonies, indicative of a potentially positive interaction between the bait (p53 or catalase) and prey (library protein), were re-streaked on SD-Leu/-Trp/-His/-Ade plates. Finally, positive clones were replica-plated on maximally selective SD-Leu/-Trp/-His/-Ade/X-α-gal medium to ensure that the colonies contained the correct phenotype. Plasmid DNA was isolated from positive clones and sequenced to identify the genes encoding the interacting proteins. The sequences were analyzed using the BLAST program available from NCBI.

14. Statistical analysis

The data are presented as means ± SE. Statistical comparisons were carried out using an unpaired *t*-test, and values of $p < 0.01$ were considered significant.

III. RESULTS

1. RRM3 interacts with catalase in vivo and in vitro

To identify novel RRM3-interacting proteins, particularly those that might be involved in regulation of ROS generation, we performed a yeast two hybrid screening of the HeLa cDNA expression library with the full length RRM3 as the bait. Yeast cells expressing the Gal4 fusion protein were transfected with the above bait. Screening of $2x10^6$ transformants resulted in the isolation of several positive clones. Sequencing of several isolated from one such positive clone identified a catalase. To further confirm catalase's interaction with RRM3, we cotransformed full length RRM3 with catalase. The transformed colonies showed ability to grow in medium lacking adenosine, histidine, tryptophan, and leucine (-AHTL) and to turn blue in a ∂Ω-galactosidase assy, while cells contransfected with the control GBK vector did not grow (data not shown).

To determine whether RRM3 would interact with catalase in a cell endogenously expressing both proteins, immunoprecipitation assays were used. We created RRM3-deficient RKO cell lines using a RRM3-targeting small interference RNA (siRNA) and immunoprecipitation assays were performed. The western blot analysis of the input (10% of the lysate used for immunoprecipitation assay) indicated the presence of catalase in both RKO (Fig. 1A) and RRM3-deficient RKO cell lysates (Fig. 1B). After RKO cells were untreated or treated with $10J/m^2$ UV irradiation, the cells were lysed, and the cellular proteins were immunoprecipitated with a RRM3-specific antibody and subjected to Western blotting with anti-catalase antibody. As shown in Fig. 1A, endogenous RRM3 bound catalase in RKO cells, and this interaction was increased after UV treatment.

However, RRM3 could not bind catalase in RRM3-deficient RKO cells (Fig. 1B). When the input was analyzed with anti-RRM3 antibody, RRM3 was clearly detected in RKO cells, but not in RRM3-deficient RKO cells. In a reciprocal coimmunoprecipitation assay with anti-catalase antibody, endogenous RRM3 readily immunoprecipitated from the cell lysates (Fig. 1C). The binding was specific, as neither RRM3 or catalase was detected in samples immunoprecipitated with rabbit IgG. These results suggest that endogenous RRM3 and catalase proteins form a complex.

To obtain further evidence for the interaction, immunofluorescence microscopy was done to determine if catalase colocalizes with RRM3. U2OS cells were untreated or teated with UV irradiation and were cosatined with anti-RRM3 and anti-catalase antibodies and results are shown in Fig. 1D. Immunofluorescence microscopy analysis revealed that RRM3 (green) and catalase (red) colocalized in cytoplasm after UV treatment. The merged images show the colocalization of catalse with RRM3 as indicated by the yellow color.

The association of RRM3 with catalase was confirmed in coimmunoprecipitation experiments using recombinant purified proteins. Recombinant purifed human RRM3 (0.5 ❍g) was incubated in the presence or absence of recombinant purified human catalase (0.5 ❍g). Then, immunoprecipitation was performed using an anti-RRM3 antibody followed by immunoblotting using anti-catalase monoclonal antibody. We found that recombinant RRM3 coimmunoprecipitated recombinant catalase (Fig. 2). These findings demonstrate that RRM3 protein bind directly to catalase.

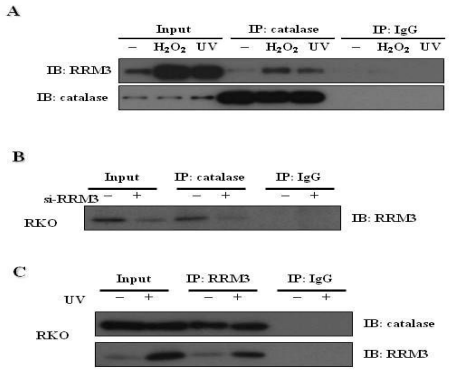
A
Input
IP: catalase
IP: IgG
– H_2O_2 UV – H_2O_2 UV – H_2O_2 UV
IB: RRM3
IB: catalase
B
Input
IP: catalase
IP: IgG
si-RRM3 – + – + – +
RKO
IB: RRM3
C
Input
IP: RRM3
IP: IgG
UV – + – + – +
RKO
IB: catalase
IB: RRM3

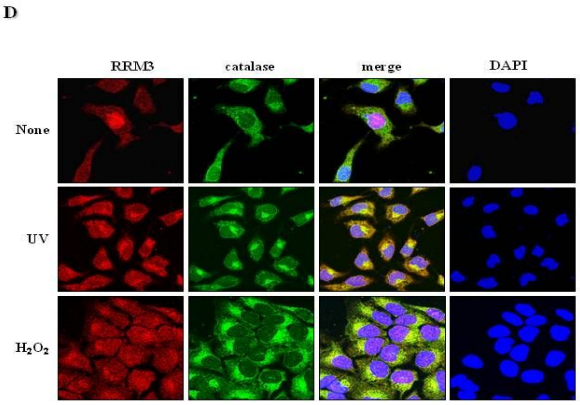
D
RRM3
catalase
merge
DAPI
None
UV
H_2O_2

Fig. 1. Interaction of RRM3 with catalase in intact cells. (a) RKO cells were untreated or treated with UV, and lysed. Proteins were immunoprecipitated from the lysates with anti-RRM3 antibody, and the immunoprecipitates were subjected to Western blot analysis with an antibody specific for catalase or RRM3. Lanes 1 and 2 contain 10% input. Normal mouse IgG was used as an immunoprecipitation control. (b) RKO cells were transfected with control or RRM3 siRNA As indicated. 48 hr after transfection, cell lysates were subjected to immunoprecipitation with anti-RRM3 antibody, and the resulting precipitates were immunoblotted with anti-catalase and anti-RRM3 antibodies. Lanes 1 and 2 contain 10% input. Normal rabbit IgG was used as an immunoprecipitation control. (c) RKO cells were untreated or treated with UV, and catalase was immunoprecipitated with anti-catalase antibody and detected with anti-RRM3 and anti-catalase antibodies. Lanes 1 and 2 contain 10% input. Normal rabbit IgG was used as an immunoprecipitation control. (d) U2OS cells were untreated or treated with UV, and stained with labeled anti-RRM3 (green) and anti-catalase (red) antibodies. Colocalization of RRM3 and catalase in cells is shown as yellow in the merged images.

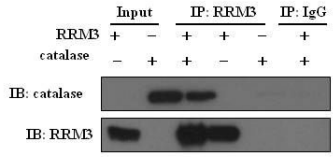

Fig. 2. RRM3 interacts with catalase in vitro. 500 ng of purified RRM3 was incubated with 1 ❍g of catalase (lane 3) or without catalase (lane 4) in PBS. Anti-RRM3 antobodies couple to protein G-sepharose beads were then added. Beads were washed and the bound immunocomplexs were analyzed by Western blot with anti-catalase and anti-RRM3 antibodies. Inputs: RRM3 (50 ng) and catalase (50 nG). Normal rabbit IgG was used as an immunoprecipitation control.

2. Catalase interacts with the C-terminal regions of RRM3

To define the region of RRM3 that is necessary for catalase binding, we made expression constructs encoding two GFP-tagged RRM3 deletion mutants, each containing N-terminal or C-terminal region: RRM3-ΔN (deleted N-terminal region, amino acids 1-150) and RRM3-ΔC (deleted C-terminal region, amino acids 151-300). Expression constructs of full length RRM3 or these deletion mutants were transfected into HEK293T cells, and immunoprecipitated them with an anti-catalase monoclonal antibody. The immune complexes were subjected to immunoblotting with a monoclonal antibody to GFP. The full length RRM3 and N-terminal truncated RRM3 (RRM3-ΔN), but not C-terminal truncated RRM3 (RRM3-ΔC), co-immunoprecipitated with catalase (Fig. 3). Control immunoprecipitation and immunoblotting from the same lystes confirmed appropriate expression from transfected plasmids, indicating that catalase associates with the C-terminal region of RRM3 in vivo.

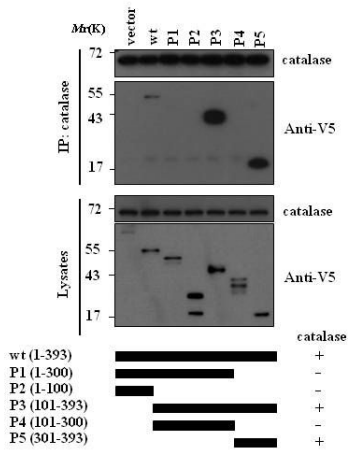

Fig. 3. RRM3 interacts with catalase via its N-terminal region. **(a)** Schematic presentation of RRM3 deletion mutants used in the study. The catalase binding property of these RRM3 constructs is summarized. (b) Lysates of HEK293T cells expressing pcDNA-DEST47T control vector (vector), GFP-tagged wild type (RRM3-WT) or GFP-tagging RRM3 deletion mutants (RRM3-C and RRM3-N) were subjected to immunoprecipitation with anti-catalase, and the lysates and resulting precipitates were subjected to immunoblot analysis with anti-GFP or anti-catalase antibodies.

3. RRM3 negatively regulates catalase activity in vivo and in vitro

The affinity of RRM3 for catalase described above prompted the search for a functional interaction between these two proteins. Since RRM3 has no catalase activity (data not shown), the possibility that it might affect the enzymatic activity of catalase was investigated. Using recombinant purified human proteins, catalase activity was tested in the presence or absence of RRM3. We found that the presence of purified RRM3 protein strongly suppressed the catalase activity in a dose-dependent manner (Fig. 4). The addition of 1, 10, 100, 1000 ng of RRM3 to the reaction mixture caused ~20, 40, 60, 80% decrease in catalase activity, respectively, as compared with RRM3 untreated control.

To explore the negative regulation of catalase by RRM3 in vivo further, we examined whether catalase activity would be inhibited when RRM3 is overexpressed. Breast cancer MCF7 cells (p53 wild type), colon cancer SW480 cells (p53 mutant) , colon cancer HCT116 $p53^{-/-}$ cells (p53 null), osteosarcoma Saos-2 (p53 null), lung cancer H1299 cells (p53 null), and lung cancer H460 cells were transiently transfected with either RRM3 expression vector or its control empty vector pcDNA3.1, and catalase activities were then measured. As show in Fig. 5A, RRM3 overexpression resulted in suppression of catalase activity in MCF7, SW480, HCT116 $p53^{-/-}$, H1299, and Saos-2 cells. Interestingly, we found that there was no catalase expression in the H460 cells (Fig. 5A, last lane). Thus, we could not detect any measurable catalase activity in H460 cells before and after RRM3 expression.

4. RRM3 increases intracellular ROS levels by inhibition of catalase activity

We next determined intracellular accumulation of ROS by flow cytometry analysis

with cell permeable ROS indicator carboxy-2`,7`-dichlorodihydrofluorescein diacetate (H_2DCFDA). This compound is nonfluorescent until intracellular esterases cleave off its lipophilic blocking groups and subsequent oxidation occurs, resulting in a charged fluorescent from trapped within the cell. We found that the level of intracellular ROS was increased in MCF7, SW480, HCT116 $p53^{-/-}$, H1299, and Saos-2 cells at 24 h after transfection of RRM3 expression vector compared with the control vector transfected cells (Fig. 5B). However, we could not detect any significant different ROS amount between control H460 cells and RRM3 expressed H460 cells (Fig. 5B, last lane). Because H460 cells is deficient in catalase, RRM3-meidated increase in ROS generation is likely to be attributed to the suppression of catalase activity.

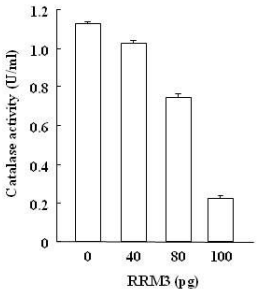

Fig. 4. Effect of RRM3 on catalase activity in vitro. The indicated amount of recombinant human RRM3 were incubated at 37 ℃ for 30 min with 1.3 U/ml of the recombinant human catalase. Catalase activities were then measured as described in Materials and Methods. The data shown are the means ± S.D. from three separate experiments.

A

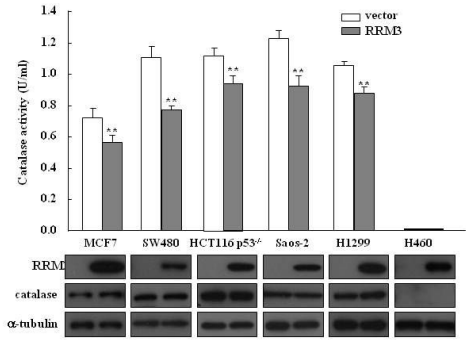
vector
RRM3
Catalase activity (U/ml)
1.4
1.2
1.0
0.8
0.6
0.4
0.2
0.0
**
MCF7
SW480
HCT116 p53-/-
Saos-2
H1299
H460
RRM3
catalase
α-tubulin

B

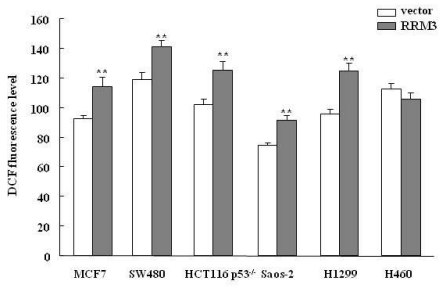
vector
RRM3
DCF fluorescence level
160
140
120
100
80
60
40
20
0
**
MCF7
SW480
HCT116 p53-/-
Saos-2
H1299
H460

Fig. 5. RRM3 suppresses catalase activity in human cancer cell lines. (a and b) MCF7, SW480, HCT116 $p53^{-/-}$, H1299, Saos-2, and H460 cells were transfected with contol or RRM3 expression vector. 24 h after transfection, ROS (a) and catalase activity (b) were then measured from three independent experiments. Cell lysates were analyzed by immunoblotting as indicated (bottom). The data shown are the means ± S.D. from three separate experiments. **, $P < 0.01$.

5. C-terminal of RRM3 required for modulation of catalase activity

It is possible that the binding of C-terminal domain of RRM3 to catalase inhibits catalase activity. If so, a RRM3 mutant that does not bind catalase should not affect. To determine if direct interaction between RRM3 and catalase is sufficient for suppression of catalase activity, the full length RRM3, N-terminal truncated RRM3 (RRM3-ΔN), or C-terminal truncated RRM3 (RRM3-ΔC) were transfected into p53 null H1299 cells. As showin in Fig 6A, the full length RRM3 and RRM3-ΔN, which retain the catalase interaction site, were able to suppress catalase activity. Accordingly, ROS production was reduced (Fig. 6B). In contrast, the RRM3-ΔC construct, which lacked the catalase binding site, did not have any effect on catalase activity as well as ROS generation. Thus, the region of 151-300 amino acids necessary for interaction with catalase is crucial for regulation of catalase activity.

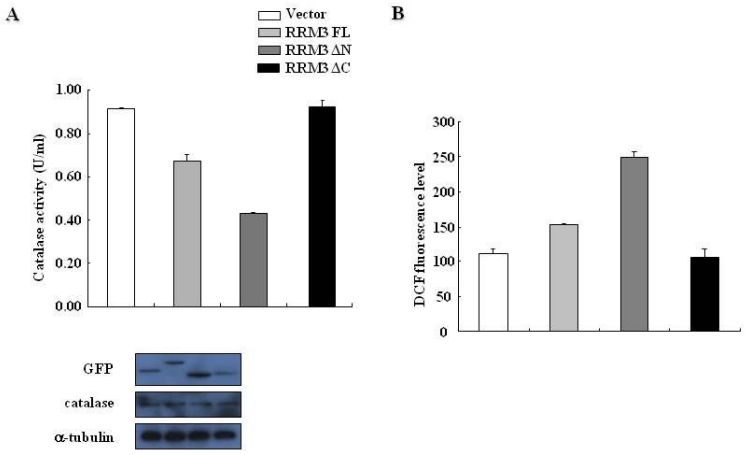

Fig. 6. C-terminal truncated RRM3 does not affect catalase activity and ROS level. Plasmids encoding GFP-tagged full length RRM3, N-terminal truncated RRM3 (RRM3-ΔN), or (RRM3-ΔC) were transfected into U2OS cells. 24 h after transfection, catalase activity (a) and ROS (b) were then measured from three independent experiments. Cell lysates were analyzed by immunoblotting as indicated (bottom). The data shown are the means ± S.D. from three separate experiments. **, $P < 0.01$.

6. RRM3-mediated suppression of catalase function is involved in RRM3-induced apoptosis in response to UV irradiation

To explore the potential role of RRM3 in the regulation of catalase activity after DNA damage, we next generated stably transfected the HCT116 $p53^{-/-}$ cells with either RRM3 expression vector or its control empty vector pcDNA. Expression of RRM3 was determined by immunoblotting the lysates from exponentially growing cells with an anti-RRM3 antibody. This clone expressed three- or fourfold elevated levels of exogenous RRM3 compared with pcDNA transfected cells (For example, Fig. 7D, left panel). The control and RRM3 overexpression HCT116 $p53^{-/-}$ cells were treated with 20 J/m^2 UV irradiation, 48 h after UV irradiation, catalase activities and ROS levels were then measured. We found that the catalase activities were ~ 20% decreased in RRM3 expressing HCT116 $p53^{-/-}$ cells after UV irradiation, compared with untreated cells (Fig. 7A). However, catalase activities did not significantly change in control HCT116 $p53^{-/-}$ cells before and after UV irradiation. Correspondingly, RRM3 expressing HCT116 $p53^{-/-}$ cells showed markedly increased ROS production in response to UV irradiation (Fig. 7B). However, ROS production in control HCT116 $p53^{-/-}$ cells was not significantly changed by UV irradiation. To determine if RRM3 overexpression has any effect on UV-induced apoptosis, the nuclei of control and RRM3 overexpressing HCT116 $p53^{-/-}$ cells were stained with a propidium iodide dye for flow cytometric detection to analyze the apoptotic sub-G1 DNA content. As shown in Fig. 7C, the RRM3 overexprssing HCT116 $p53^{-/-}$ cells showed significantly increases in apoptotic sub-G1 DNA content in response to UV irradiation. The control HCT116 $p53^{-/-}$ cells showed an apoptotic sub-G1 DNA content

ranging from 7.08% to 12.96% in response to 20 to 40 J/m^2 UV irradiation. In contrast, the RRM3 overexprssing HCT116 $p53^{-/-}$ cells showed significantly increases in apoptotic sub-G1 DNA content from 11.53% to 23.26% at the same conditions. Because the activation of casapse is one of the major processes in ROS-induced apoptosis, we tested the induced level of caspase-3/7, the key apoptotic caspases, in control and RRM3 expressing HCT116 $p53^{-/-}$ cells by Western blot analysis. There was no significant different in the level of procaspase-3 and procaspase-7 between control and RRM3 overexpressing HCT116 $p53^{-/-}$ cells (Fig. 7D). However, although none of the active processed products of both enzymes were detected in the control cells up to 24 h after 10 J/m^2 UV irradiation, the cleavage of procaspase-3/7 into the active subunits was clearly observed in the RRM3 overexpressing cells from 24 h after UV irradiation. These results led us to study whether catalase suppresses RRM3-induced apoptosis. To do this experiments, HCT116 $p53^{-/-}$ cells stably transfected with control or RRM3 expression vectors were infected with Ad-GFP or Ad-catalase, and apoptosis was examined. We observed that UV-induced apoptosis (Fig. 8A) and caspase-3/7 cleavage (Fig. 8B) were significantly decreased in catalase-overexpressing cells. Therefore, the activation of RRM3 in response to DNA damage in p53-proficient cells may lead to the suppression of catalase activity, resulting in increased ROS levels, which might play an important role in p53-mediated apoptosis.

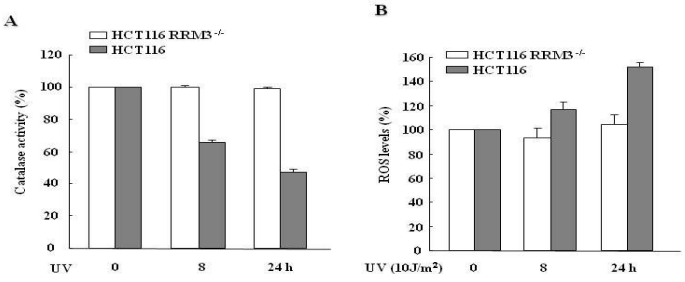
A
HCT116 RRM3-/-
HCT116
Catalase activity (%)
120
100
80
60
40
20
0
UV
0
8
24 h
B
HCT116 RRM3-/-
HCT116
ROS levels (%)
160
140
120
100
80
60
40
20
0
UV (10J/m2)
0
8
24 h

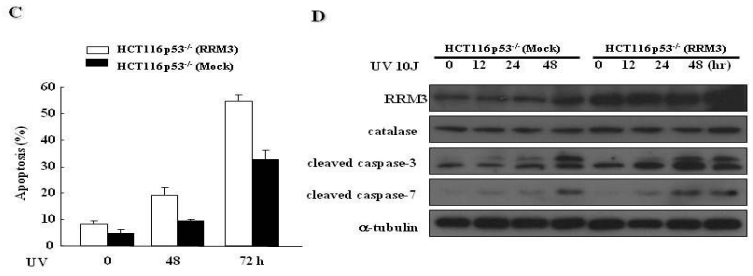
C
HCT116p53-/- (RRM3)
HCT116p53-/- (Mock)
Apoptosis (%)
60
50
40
30
20
10
0
UV
0
48
72 h
D
HCT116p53-/- (Mock)
HCT116p53-/- (RRM3)
UV 10J
0 12 24 48
0 12 24 48 (hr)
RRM3
catalase
cleaved caspase-3
cleaved caspase-7
α-tubulin

Fig. 7. The role of RRM3 in UV-induced apoptosis of HCT116 $p53^{-/-}$ cells. (a and b) Mock and RRM3 expressing HCT116 $RRM3^{-/-}$ cells were irradiated with 20J/m^2 UV. 48 h after irradiation, and catalase activities (a) and ROS levels (b) were then determined. The measured catalase activity and ROS are expressed as percentage levels over untreated cells. The data shown are the means ± S.D. from three separate experiments. **, $P < 0.01$. (c) Mock and catalase expressing HCT116 $p53^{-/-}$ cells were treated with 0, 20, and 40 J/m^2 UV irradiation. 48 h after irradiation, apoptotic cells (Sub-G1) according to DNA content (PI staining) were analyzed. The data shown are the means ± S.D. from three separate experiments. **, $P < 0.01$. (d) Mock and catalase expressing HCT116 $p53^{-/-}$ cells were untreated or treated with 10 J/m^2 UV irradiation for the indicated times. The cell lysates were blotted with indicated antibodies. Cleavage of caspase-3 and caspase-7 was detected as indicators of apoptosis.

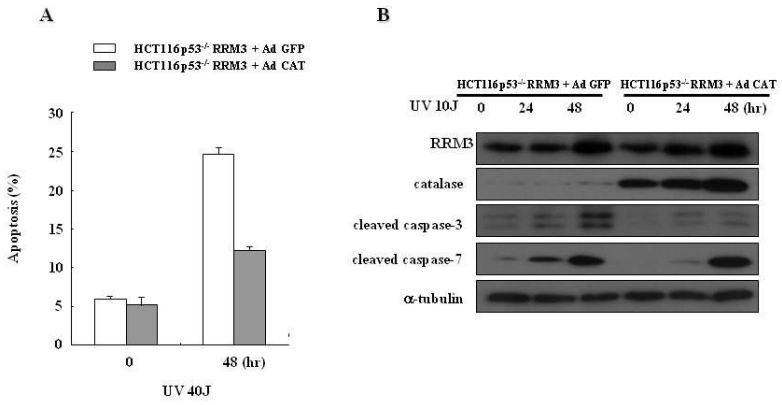

Fig. 8. The overexpression of catalase inhibits apoptotic cell death in RRM3 expressing HCT116 p53$^{-/-}$cells. (a) Mock and catalase expressing HCT116 p53$^{-/-}$ cells were infected with either Ad-RRM3 or Ad-GFP for 24 h, and cells were then treated with 0, 20, and 40 J/m^2 UV irradiation. 48 h after irradiation, apoptotic cells (Sub-G1) according to DNA content (PI staining) were were analyzed. The data shown are the means ± S.D. from three separate experiments. **, $P < 0.01$. (b) Mock and catalase expressing HCT116 p53$^{-/-}$ cells were infected with either Ad-RRM3 or Ad-GFP for 24 h, and cells were then untreated or treated with 10 J/m^2 UV irradiation for the indicated times. The cell lysates were blotted with indicated antibodies. Cleavage of caspase-3 and caspase-7 was detected as indicators of apoptosis.

IV. DISCUSSSION

It is known that the extent of p53-induced apoptosis can be modulated by decreasing or increasing the extent of oxidative stress, which triggers the activation and nuclear translocation of p53. However, recent evidence suggests that ROS is not only an upstream activator of the p53 pathway, but it is also a critical component of the downstream mediator of p53-dependent apoptosis, because overexpression of wild type p53 produces ROS in association with apoptosis (18). Activated p53 increases cellular ROS levels by enhancing the transcription of proapoptotic genes. These genes include Bax, PIGs (p53-induced genes), Noxa, APAF-1, PUMA. Upon its activation following DNA damage, p53 can activate several genes that result in increased ROS generation, which contributes to the induction of apoptosis in cells with unrepaired DNA damage (4, 18-21). The induction of apoptosis is central to the tumor-suppressive activity of p53 (22-23). However, physiological levels of p53 can also upregulate antioxidant genes, including glutathione peroxidase, mitochondrial superoxide mutase 2, mammalian sestrin homologs SENS1 and SENS2, and tumor protein 53-induced nuclear protein, and this antioxidant function of p53 is important in preventing oxidative stress-induced DNA damage and tumor development under low-stress conditions (24-31). Thus, p53 has opposing roles in the regulation of ROS, depending on the nature and intensity of the stress and on the cellular context (12). The precise molecular mechanisms of the balance between pro-oxidant and antioxidant states caused by p53 are not completely understood.

In an attempt to identify downstream targets of p53, Polyak and colleagues used colorectal cancer line DLD-1, which undergo apoptosis in response to exogenous p53

expression, to evaluate the patterns of gene expression upon adenoviral p53-induction (4). Employing serial analysis of gene expression (SAGE) they found that transcription was induced (>10 fold) for 14 different mRNA's, of which 13 were not previously known to be p53 targets in human cells. These p53 inducible genes (PIGs) were given number 1-13, of which PIGs predicted to encode proteins that could generate or response to oxidative stress. Although, the downstream effects of ROS production are not well understood, it is clear that ROS does play a role in the mechanisms of cell death, because blocking its production inhibits apoptosis (17, 32-33). The discovery of PIG genes strongly suggests that oxidative damage of mitochondria might play an important role in the p53-induced apoptosis. These were the first clear connection between p53 and ROS generation.

Of particular interest is RRM3, which shares sequence similarity with NADPH-quinine oxidoreductase (NQO), therefore can influence the production of intracellular ROS. RRM3 promoter contains p53 response element, thus RRM3 is induced by p53 (5). RRM3 expression can also be elicited by p63 and p53 (6), which are able to induce apoptosis in a p53-independent manner (7). UV irradiation induces alternative splicing of the *RRM3* pre-mRNA to produce a splice variant protein that is degraded rapidly by the proteasome degradation pathway, implicating a novel paradigm between the cellular DNA damage response and control of alternative splicing (34). Additionally, heterogeneous nuclear ribonuclear protein A1 and A2 is contributed to the normal alternative splicing of RRM3 but is not involved in the UV-inducible alternative splicing of this transcript, suggesting that the different mechanisms mediating normal and UV-inducible alternative spicing of RRM3 may exist (35). Moreover, RRM3 expression precedes the appearance of ROS in

p53-induced apoptosis, and certain p53 mutants capable of inducing cell cycle arrest but not apoptosis retain the ability to activate target genes such as cyclin-dependent kinase inhibitor p21, but not RRM3.Thus RRM3 may be one of the factors involved in p53-induced apoptosis through ROS generation.

In the present study, we used a yeast two-hybrid system to identify catalase as a RRM3-binding protein. This interaction also occurs in cultured human cells, as shown by co-immunoprecipitation and co-localization of endogenous catalase with RRM3. The RRM3-catalse interaction is likely to be direct, as shown by an in vitro coimmunoprecipitation assay with recombinant. Importantly, we found that the expression of RRM3 is sufficient to produce ROS and the ROS generation is attributable to a suppression of catalase activity. Recently, Porter et al demonstrated that RRM3 exhibited quinone reductase activity using NADPH as a cofactor, and identified substrate- and cofactor-binding sites, with residues fully conserved from bacteria and human (36). They also have shown that in vitro RRM3 activity generates ROS, and that RRM3 overexpression in cells leads to ROS generation, which is dependent on active enzyme or at least on protein able to bind cofactor. Therefore they suggested that RRM3 action on ROS generation and, probably, on apoptosis is through its enzymatic activity with an endogenous substrate of the quinone type. However, we found that ROS production in H460 cells, which are deficient in catalase, was not affected by RRM3 overexpression. In addition, ROS production in catalase-expressing H460H460 cells infected with Ad-RRM3 was increased intracellular ROS levels. Moreover, a region between amino acids 1 and 206 of RRM3, which does not bind catalase, did not have effect on the ROS level. Thus,

although quinone reductase activity of RRM3 is involved in the ROS generation, it is our belief that RRM3-mediated decrease in catalase activity is main cause of RRM3-induced enhanced ROS generation.In summary, our findings clearly demonstrate that RRM3 regulates ROS levels through direct protein–protein interactions. Specifically, RRM3 interact with catalase to negatively regulate catalase activity. In severe genotoxic stress, high levels of RRM3 decrease catalase activity, and thereby shift the intracellular environment toward oxidant conditions, causing apoptotic cell death. Thus, depending on the intensity of the stress and the specific interacting partners, RRM3 acts as a pro-oxidant. This study provides direct experimental evidence that the pro-oxidant functions of RRM3 are tightly linked to the regulation of catalase activity in mammalian cells.

V. REFERENCES

1. Oren M. Decision making by p53: life, death and cancer. Cell Death Differ 2003;10:431-42.

2. El-Deiry WS. The role of p53 in chemosensitivity and radiosensitivity. Oncogene 2003;22:7486-95.

3. Giaccia AJ, Kastan MB. The complexity of p53 modulation: emerging patterns from divergent signals. Genes Dev 1998;12:2973-83.

4. Polyak K, Xia Y, Zweier JL, Kinzler KW, Vogelstein B. A model for p53-induced apoptosis. Nature 1997;389:300-5.

5. Contente A, Dittmer A, Koch MC, Roth J, Dobbelstein M. A polymorphic microsatellite that mediates induction of RRM3 by p53. Nat Genet 2002;30:315-20.

6. Bergamaschi D, Samuels Y, Jin B, Duraisingham S, Crook T, Lu X. ASPP1 and ASPP2: common activators of p53 family members. Mol Cell Biol 2004;24:1341-50.

7. Moll UM, Slade N. p63 and p73: roles in development and tumor formation. Mol Cancer Res 2004;2:371-86.

8. Roth J, Koch P, Contente A, Dobbelstein M. Tumor-derived mutations within the DNA-binding domain of p53 that phenotypically resemble the deletion of the proline-rich domain. Oncogene 2000;19:1834-42.

9. Venot C, Maratrat M, Dureuil C, Conseiller E, Bracco L, Debussche L. The requirement for the p53 proline-rich functional domain for mediation of apoptosis is correlated with specific RRM3 gene transactivation and with transcriptional repression. EMBO J 1998;17:4668-79.

10. Zhu J, Jiang J, Zhou W, Zhu K, Chen X. Differential regulation of cellular target genes by p53 devoid of the PXXP motifs with impaired apoptotic activity. Oncogene 1999;18:2149-55.

11. Tanaka T, Ohkubo S, Tatsuno I, Prives C. hCAS/CSE1L associates with chromatin and regulates expression of select p53 target genes. Cell 2007;130:638-50.

12. Liu B, Chen Y, St Clair DK. ROS and p53: a versatile partnership. Free Radic Biol Med 2008;44:1529-35.

13. Valko M, Rhodes CJ, Moncol J, Izakovic M, Mazur M. Free radicals, metals and antioxidants in oxidative stress-induced cancer. Chem Biol Interact 2006;160:1-40.

14. Valko M, Leibfritz D, Moncol J, Cronin MT, Mazur M, Telser J. Free radicals and antioxidants in normal physiological functions and human disease. Int J Biochem Cell Biol 2007;39:44-84.

15. Terada LS. Specificity in reactive oxidant signaling: think globally, act locally. J Cell Biol 2006;174:615-23.

16. Ozben T. Oxidative stress and apoptosis: impact on cancer therapy. J Pharm Sci 2007;96:2181-96.

17. Buttke TM, Sandstrom PA. Oxidative stress as a mediator of apoptosis. Immunol Today 1994;15:7-10.

18. Johnson TM, Yu ZX, Ferrans VJ, Lowenstein RA, Finkel T. Reactive oxygen species are downstream mediators of p53-dependent apoptosis. Proc Natl Acad Sci U S A 1996;93:11848-52.

19. Liu G, Chen X. The ferredoxin reductase gene is regulated by the p53 family and

sensitizes cells to oxidative stress-induced apoptosis. Oncogene 2002;21:7195-204.
20. Macip S, Igarashi M, Berggren P, Yu J, Lee SW, Aaronson SA. Influence of induced reactive oxygen species in p53-mediated cell fate decisions. Mol Cell Biol 2003;23:8576-85.
21. Donald SP, Sun XY, Hu CA, et al. Proline oxidase, encoded by p53-induced gene-6, catalyzes the generation of proline-dependent reactive oxygen species. Cancer Res 2001;61:1810-5.
22. Schmitt CA, Fridman JS, Yang M, Baranov E, Hoffman RM, Lowe SW. Dissecting p53 tumor suppressor functions in vivo. Cancer Cell 2002;1:289-98.
23. Vousden KH, Prives C. Blinded by the Light: The Growing Complexity of p53. Cell 2009;137:413-31.
24. Matoba S, Kang JG, Patino WD, et al. p53 regulates mitochondrial respiration. Science 2006;312:1650-3.
25. Sablina AA, Budanov AV, Ilyinskaya GV, Agapova LS, Kravchenko JE, Chumakov PM. The antioxidant function of the p53 tumor suppressor. Nat Med 2005;11:1306-13.
26. Hussain SP, Amstad P, He P, et al. p53-induced up-regulation of MnSOD and GPx but not catalase increases oxidative stress and apoptosis. Cancer Res 2004;64:2350-6.
27. Meiller A, Alvarez S, Drane P, et al. p53-dependent stimulation of redox-related genes in the lymphoid organs of gamma-irradiated−mice identification of Haeme-oxygenase 1 as a direct p53 target gene. Nucleic Acids Res 2007;35:6924-34.
28. Bensaad K, Tsuruta A, Selak MA, et al. TIGAR, a p53-inducible regulator of glycolysis and apoptosis. Cell 2006;126:107-20.

29. Budanov AV, Sablina AA, Feinstein E, Koonin EV, Chumakov PM. Regeneration of peroxiredoxins by p53-regulated sestrins, homologs of bacterial AhpD. Science 2004;304:596-600.

30. Chen W, Sun Z, Wang XJ, et al. Direct interaction between Nrf2 and p21(Cip1/WAF1) upregulates the Nrf2-mediated antioxidant response. Mol Cell 2009;34:663-73.

31. Cano CE, Gommeaux J, Pietri S, et al. Tumor protein 53-induced nuclear protein 1 is a major mediator of p53 antioxidant function. Cancer Res 2009;69:219-26.

32. Carmody RJ, Cotter TG. Signalling apoptosis: a radical approach. Redox Rep 2001;6:77-90.

33. Quillet-Mary A, Jaffrezou JP, Mansat V, Bordier C, Naval J, Laurent G. Implication of mitochondrial hydrogen peroxide generation in ceramide-induced apoptosis. J Biol Chem 1997;272:21388-95.

34. Nicholls CD, Shields MA, Lee PW, Robbins SM, Beattie TL. UV-dependent alternative splicing uncouples p53 activity and RRM3 gene function through rapid proteolytic degradation. J Biol Chem 2004;279:24171-8.

35. Nicholls CD, Beattie TL. Multiple factors influence the normal and UV-inducible alternative splicing of RRM3. Biochim Biophys Acta 2008;1779:838-49.

36. Porte S, Valencia E, Yakovtseva EA, et al. Three-dimensional structure and enzymatic function of proapoptotic human p53-inducible quinone oxidoreductase RRM3. J Biol Chem 2009;284:17194-205.